Protecting Group Free Synthesis of Glyco-Nanoparticles using Amino-oxy Terminated Polymer Ligands

Antonio Laezza,[†,‖,∇] *Panagiotis G. Georgiou,*[†,∇] *Sarah-Jane Richards,*[†] *Alexander N. Baker,*[†] *Marc Walker,*[§] *Matthew I. Gibson**[,†,‡]

[†] Department of Chemistry, University of Warwick, Gibbet Hill Road, Coventry, CV4 7AL, UK

[‡] Warwick Medical School, University of Warwick, Gibbet Hill Road, Coventry, CV4 7AL, UK

[§] Department of Physics, University of Warwick, Gibbet Hill Road, Coventry, CV4 7AL, UK

[‖]Current address. Department of Sciences, University of Basilicata, Potenza, Italy, I-85100

[∇]These authors contributed equally to this work

**Corresponding Author:* m.i.gibson@warwick.ac.uk

ABSTRACT

Glyco-materials display enhanced binding affinity to carbohydrate binding proteins due to the non-linear enhancement associated with the cluster glycoside effect. Gold nanoparticles bearing glycans have attracted significant interest in particular. This is due to their versatility, highly-tuneable gold cores (size and shape), and their application in biosensors and diagnostic tools. However, conjugating glycans onto these materials can be challenging: necessitating either multiple protecting group manipulations, or the use of only simple glycans. This results in limited structural diversity compared to glyco-arrays which can include 100's of glycans. Here we report a method to generate glyconanoparticles from unprotected glycans by conjugation to polymer tethers bearing terminal amino-oxy groups, which are then immobilised onto gold nanoparticles. Using an isotope labelled glycan, the efficiency of this reaction was probed in detail to confirm conjugation, with 25 % of end-groups being functionalised, predominantly in the ring-closed form. Facile post-glycosylation purification is achieved by simple centrifugation/washing cycles to remove excess glycan and polymer. This streamlined synthetic approach may be particularly useful for the preparation of glyconanoparticle libraries using automation, to identify hits to be taken forward using more conventional synthetic methods.. Exemplar lectin binding studies were undertaken to confirm the availability of the glycans for binding and show this is a powerful tool for rapid assessment of multivalent glycan binding.

INTRODUCTION

Glycan-lectin interactions drive a range of biological signalling events, despite the intrinsically low affinity between a single glycan and a lectin partner.[1–3] Glycans are displayed in multivalent formats on cell surfaces, leading to a non-linear increase in binding affinity termed the "cluster glycoside effect". This results in observed affinity (K_d's) increases from mM to nM or lower.[1,4] Considering this, there has been major interest in the development of synthetic materials (polymers, particles and surfaces) that mimic the glycocalyx[5] through multivalent display.[6–8] For example, multivalent glycopolymers can act as decoys to prevent/inhibit the initial engagements between pathogens and their hosts.[9–13] Kiessling and co-workers have shown that glycopolymer architecture is crucial to their overall binding affinity and function,[8] and used to understand how viruses are routed into dendritic cells.[14] Percec and co-workers have used dendrimers to probe architectural effects in galectin affinity and selectivity.[15] While, the sequence and heterogeneity of multivalent displays is also emerging as a crucial tool to control affinity/selectivity.[16,17]

Although there has been much interest in glycomaterials, the simplest monosaccharides (e.g. glucose, mannose, galactose) are still the most widely used; often to reduce the number of protection/deprotection steps and to enable the installation of reactive (orthogonal) units typically at the reducing (anomeric) position. This narrow chemical space is in stark contrast to micro-arrays,[18] which can contain 100's of complex glycans: a level of diversity not fully embraced in glyconanomaterials. In addition to using functionalized glycans,[19] native (reducing) glycans have been captured directly using hydrazide[20] and amino-oxy[21] chemistries in array format. Alternatively, glycans have been captured by reductive amidation onto lipids (neo-glycolipid arrays), suitable for printing.[22]

The chemical synthesis of glycomaterials is often non-trivial with larger scales, compared to arrays for example, being essential. Cameron and co-workers have synthesized glycosylated

methacrylates, which required multiple steps and column purification before polymerization.[23] This has led to post-polymerization modification emerging as a useful technique.[24] For example, Haddleton and co-workers used glycosyl azides to modify alkyne-functionalized polymers in azide-alkyne click cycloadditions.[25] Other examples of the deployment of click-type reactions include; thiol-ene,[26] thiol-yne,[27] thiol-chloro,[28] activated esters,[29,30] or thiolactones.[31] Whilst convenient, the bottleneck is often the installation of the reactive handle onto the glycan. To overcome this challenge, Fairbanks[32] and Tanaka[33] have used imidazolinium salts to introduce azides at the reducing terminus directly from reducing glycans, allowing 1-pot 2-step glycosylations. Furthermore, strategies for the introduction of a thiol at the reducing terminus (for 'thiol-ene' reactions) have also been reported in protecting-group free syntheses.[34] For monosaccharides, (e.g. mannose, glucose) these additional steps are often trivial, while for more complex branched glycans that are only available in small quantities this is more challenging, plus azide reagents require careful handling. It should be noted that automated solid-phase oligosaccharide syntheses present opportunities for installation of conjugation 'handles'.[35] Yan et al. have developed perfluorophenyl azides, for photochemical glycan capture onto nanomaterials, but this does not give precise control over the position of the conjugation around the glycan ring.[36]

An appealing strategy for glycan conjugation is to exploit the hemiacetal equilibrium at the terminus of reducing glycans, conjugating to the aldehyde form. Glyconanoparticle/polymer libraries have been prepared using hydrazide functional polymers,[37–39] but there are significant challenges. The hydrazone bond is intrinsically dynamic so (depending on pH) the glycans can detach and exchange in a dynamic equilibrium.[40] Furthermore, the hydrazone linkage is an equilibrium between a ring-opened and ring-closed form, resulting in increased heterogeneity. Chemical reduction (using e.g. $NaBH_4$) can increase stability but adds another step to the process. To overcome this, amino-oxy conjugates have emerged as alternatives due to their

higher stability against hydrolysis[41,42] and, at equilibrium exist in greater proportions as ring-closed structures (more like the native linkages) compared to hydrazides.[43,44] There is therefore a significant opportunity to develop new chemical tools to enable the assembly of glyconanoparticle libraries using more complex oligosaccharides and preferably using methods that are compatible with automation to mimic the complexity of current (2-D) arrays.

Considering the above, this manuscript describes a synthetic approach to obtain glycosylated, multivalent nanoparticles, that does not require any glycan protecting group chemistry, using amino-oxy terminated polymers. The synthesis of amino-oxy terminated polymers by reversible addition-fragmentation chain-transfer (RAFT) polymerization is optimized and the conjugation of a representative panel of mono-, di- and tri- saccharides are captured and installed onto gold nanoparticles (AuNPs). Lectin binding assays confirmed the presentation of the glycans, and their availability for binding. This methodology will be especially useful for assembling libraries from native glycans and to facilitate the development of automated glyconanoparticle synthesis procedures.

RESULTS AND DISCUSSION

The key aim of this study was to develop a synthetic methodology for the conjugation of reducing (protecting-group free) glycans in aqueous solution directly onto polymer ligands; for subsequent assembly into glyco-nanomaterials, to screen for protein binding. The synthetic strategy devised is shown in Figure 1. The targeted amino-oxy group cannot be incorporated into a RAFT agent as its nucleophilicity would interact with the RAFT agent's thiocarbonyl motifs, therefore a post-polymerization modification strategy was employed. This involved the installation of a phthalimide protected amino-oxy group onto a RAFT-derived poly(*N*-hydroxyethyl acrylamide) (pHEA) scaffold by displacement of the pentafluorophenol group, followed by immobilization onto pre-formed citrate stabilised gold nanoparticles (AuNPs). pHEA was selected as the polymer linker guided by our previous studies.[37,45,46] pHEA is water soluble, uncharged (to prevent non-specific protein capture) and leads to a terminal secondary thiol for gold nanoparticle conjugation. Furthermore, the acrylamide, rather than acrylate, ensures there are no thiolactam side-reactions.[47] It is important to note that the extent of RAFT agent cleavage upon amine treatment is dependent on the relative excess of amine added (Figures S4, S5), but that even with incomplete cleavage the trithioester still assembles on the gold surface.[48]

The RAFT agent, pentafluorophenyl 2-(dodecylthiocarbonothioylthio)-2-methylpropionic acid (PFP-DMP), was used to target a degree of polymerization of 25, which is optimal for coating 20 nm gold nanoparticles for non-aggregative assays (due to the choice of binding assay, see later).[37,46] The polymer was characterized by ^{1}H and ^{19}F-NMR (Figure 2), and infrared spectroscopy (FT-IR) (Figure 3A). Size exclusion chromatography (SEC) showed a narrow molecular weight distribution (Figure S3, Supporting Info), as expected for RAFT polymerisation with this monomer ($M_{n,\,NMR}$ = 3,400 g mol^{-1}, $M_{n,\,SEC}$ = 4,950 g mol^{-1}, $Đ_M$ = 1.17)

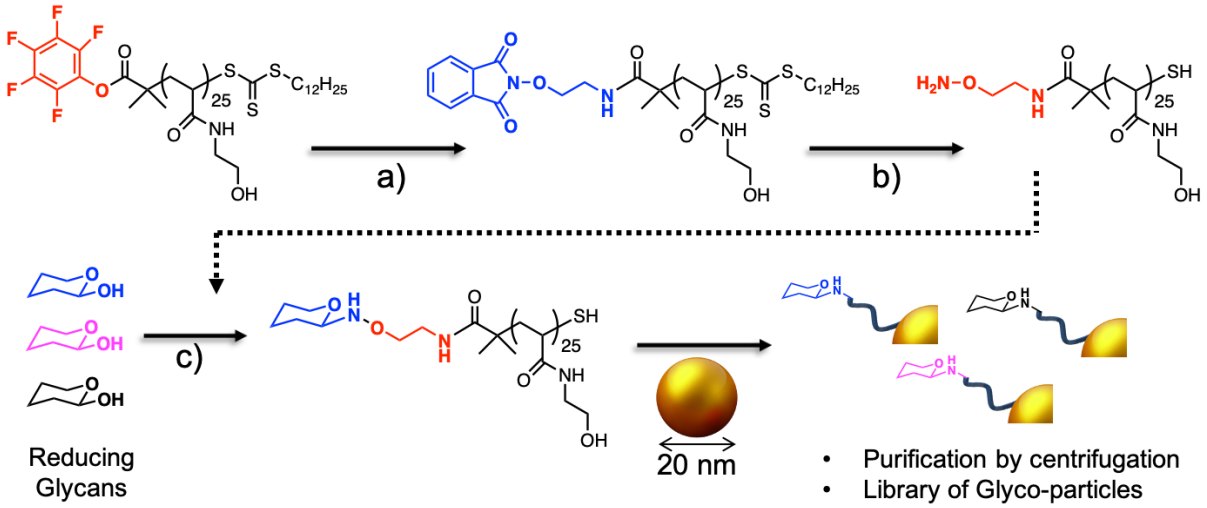

Figure 1. Overall synthetic scheme showing convergent approach to capturing glycans and subsequent immobilization. (a) Et_3N, DMF, T = 50 °C, overnight; (b) $N_2H_4 \cdot H_2O$ 50-60%, DMF, T = 50 °C, overnight; (c) acetate buffer pH = 5.5, 0.5% aniline, T = 50 °C, overnight.

As a next step, it was necessary to obtain the protected amino-oxy precursor, with amine functionality to enable installation onto the polymer. The chloride salt of 2-(2-amino-ethoxy)-isoindole-1,3-dione (**2**) was synthesized (Scheme 1) through *N*-Boc-ethanolamine coupling with *N*-hydroxyphthalimide,[49] as a modified Mitsunobu reaction[50] where a primary alcohol is transformed into the *O*-alkyl phthalimide (**1**) followed by *N*-Boc deprotection with HCl. The success of the reaction was confirmed by ESI-MS, ^{1}H-NMR and ^{13}C-NMR confirming the presence of the ammonium salt peak, attributed to the singlet ~ δ 8.30 (Figures S1 and S2, Supporting Info).

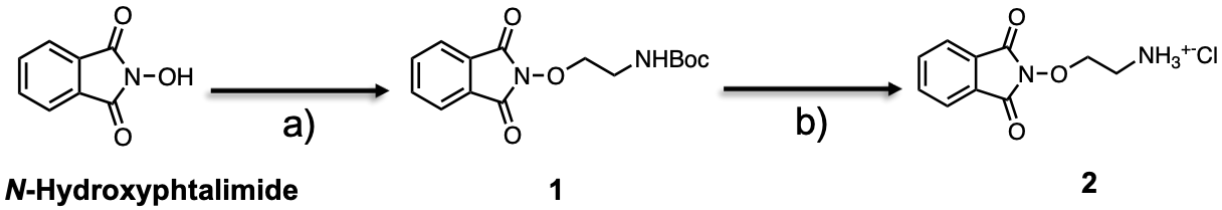

Scheme 1. (a) *N*-Boc-Ethanolamine, DIAD, PPh_3, THF, R.T.; (b) EtOAc, HCl (4M), quant., over two steps from *N*-hydroxyphthalimide.

Polymer (PFP-pHEA$_{25}$) was reacted with **2** displacing the PFP-group. Infrared spectroscopy confirmed the conversion from pentafluorophenol ester to amide by the shift of the peak at ~ 1750 cm^{-1} to ~ 1720 cm^{-1} and by the disappearance of the C-F stretch at ~ 1000 cm^{-1} (Figure 3A). ^{19}F-NMR showed quantitative removal of the PFP group (Figure 2), and ^{1}H-NMR the incorporation of aromatic proton peaks (δ 8.2–7.4 ppm) belonging to the *N*-phthaloyl group (Figure S4, Supporting Info). Finally, the *N*-phthaloyl group was removed using hydrazine to afford the amino-oxy terminated polymer (amino-oxy-pHEA$_{25}$), as shown in Figure 1 (residual RAFT agent is also cleaved). Since α and β methylene ^{1}H signals from the amino-oxy linker overlap with those of the polymer, the presence of the amino-oxy was confirmed by ^{1}H-NMR from the presence of peak ~ 8.30 ppm and from the disappearance of aromatic peaks (Figure S5, Supporting Info). FT-IR showed a peak at ~ 926 cm^{-1} belonging to the stretching of N-O and the disappearance of out of plane C-H band stretches of the aromatic ring at ~ 816 cm^{-1} (Figure 3B).

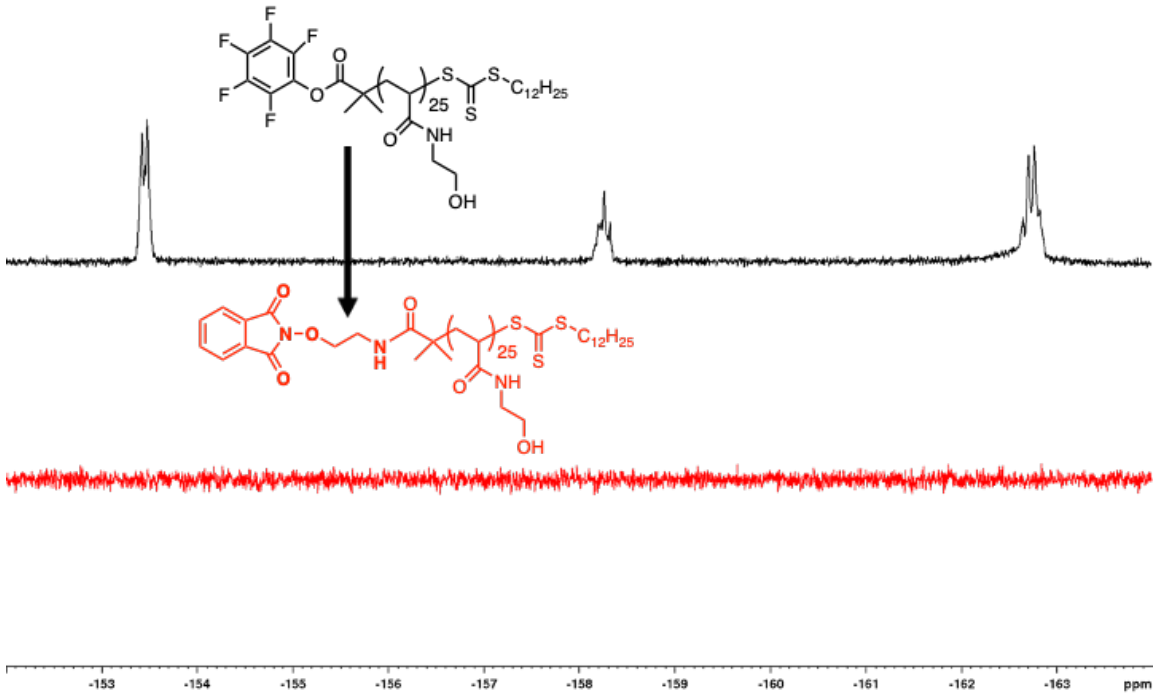

Figure 2. ^{19}F-NMR spectra of PFP-pHEA$_{25}$ (black) and 2-(2-amino-ethoxy)-isoindole-1,3-dione modified -pHEA$_{25}$ (red) (400 MHz, methanol-d_4).

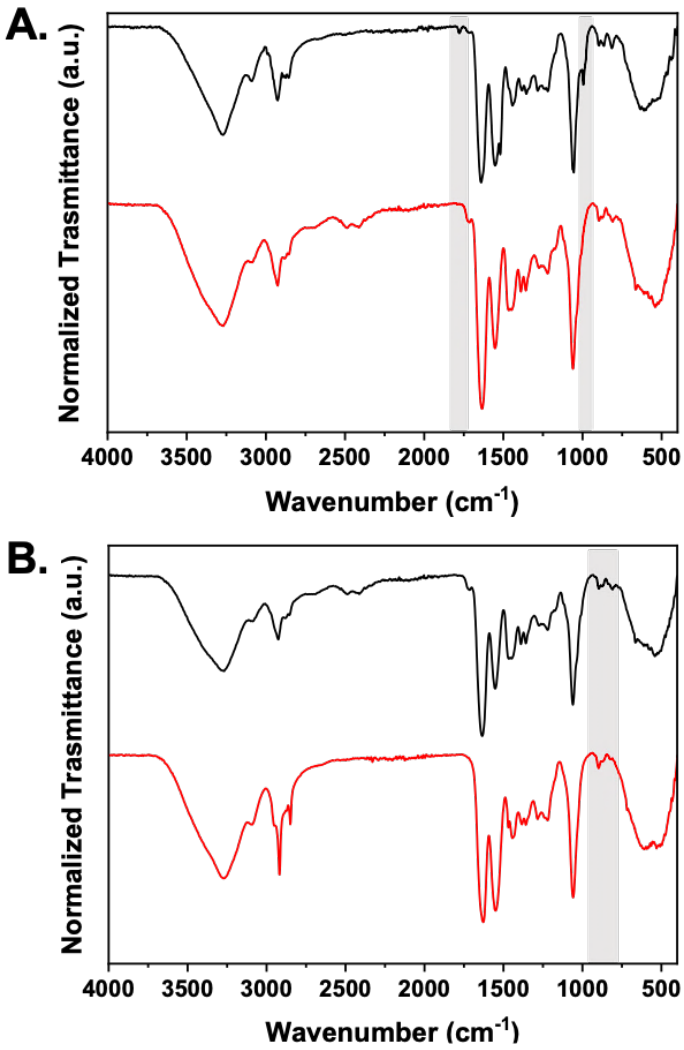

Figure 3. FT-IR spectra for end-group modifications. A) PFP-terminated $pHEA_{25}$ in black and following displacement reaction with phthalimide (red); B) phthalimide-terminated $pHEA_{25}$ (black) and after reduction with hydrazine (red).

With the amino-oxy terminated polymer prepared, glycosylation could be explored. The evaluation of glycosylation at a polymer end-group can be challenging due to the low effective concentration and the need for ^{13}C-NMR to distinguish between the possible tautomeric forms.[51] Rather than using model small molecules, which may lead to over-estimation of reaction efficiency by not reproducing the steric hindrance of the polymer chain ends, we employed ^{13}C-enriched [1-^{13}C]-D-glucose to increase signal for the trial glycosylations. Glycosylation was evaluated using amino-oxy-$pHEA_{25}$ and [1-^{13}C]-D-glucose in 1:20 molar ratio in a D_2O/acetate buffer (pD = 5.5) containing 1 mM aniline as nucleophilic catalyst[52] overnight at 50 °C.

Figure 4 shows a quantitative ^{13}C-NMR spectrum of the glycosylation mixture, acquired using an inverse gated proton-decoupling pulse sequence to minimize NOEs. In the anomeric region two peaks (δ 91.1 and 90.5 ppm) can be assigned to the C1 of β-linked [1-^{13}C]-Glc unit. This was confirmed by the HSQC spectrum (Figure S7) showing cross-peaks ($\delta_{H/C}$ = 4.03/91.1 and 4.03/90.5 ppm) with a proton in a typical anomeric region displaying $^{3}J_{1,2}$ = 8.80 Hz, characteristic of a β-linkage. The two separate β-anomer carbon peaks are explained by the resonance of ^{13}C nuclei close to secondary amino groups undergoing deuterium-induced isotope shifts of NH/ND exchange. This is slower[53] than OH to OD, leading to a detection of the amino sugar as separate signals.[54] The formation of the β-anomer is expected due to the equatorial C-2 configuration in glucose, whereas axial C-2 stereoisomers (e.g. mannose) would be expected to lead to α-configuration.[55,56]

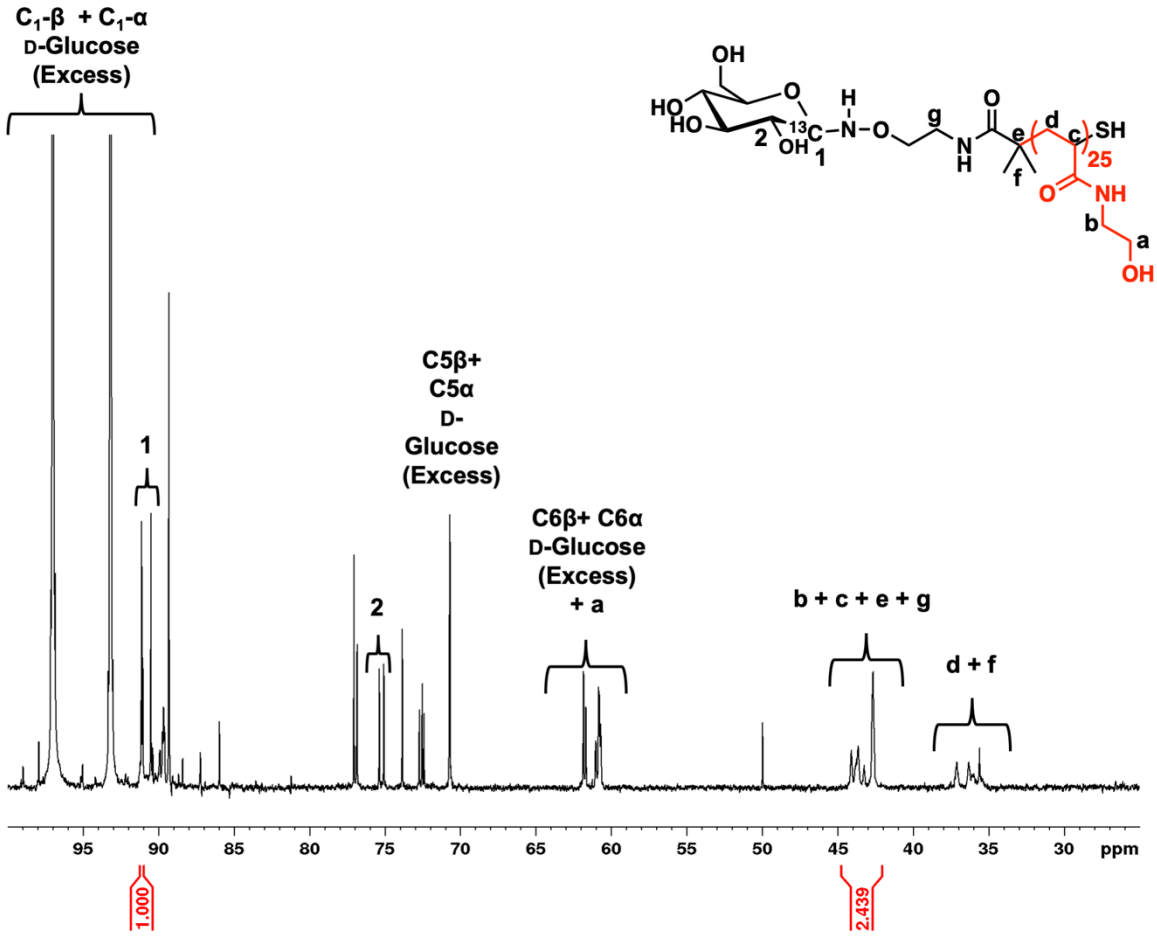

Figure 4. Quantitative ^{13}C-NMR spectrum of amino-oxy-pHEA$_{25}$ glycosylation crude mixture (600 MHz, acetate buffer 100 mM, aniline 1mM, D_2O pD =5.5).

If ring-opened glycans were present (as opposed to ring-closed), H-1 peaks would be expected in the regions δ 7.80-7.50 and δ 7.00-6.70 ppm, which partially overlap with the aniline catalyst.[52,57] Figure 5 shows a series of ^{1}H-NMR spectra of each component used in the reaction, highlighting that there were no peaks in any conditions above 7.50 ppm. Figure 5A shows the [1-^{13}C]-D-glucose alone, with no aromatic peaks. Figure 5B shows [1-^{13}C]-D-glucose in the reaction buffer showing a characteristic peak at δ 6.8 ppm, due to the aniline-glucose ring-closed adduct.[58] The polymer in the reaction buffer (with aniline) did not show this peak, Figure 5C. Figure 5D shows that in the complete reaction mixture only the ring-closed peak is present, due to the thermodynamic favourability of the closed form when using amino-oxy conjugation, plus the use of excess glycan.

Guided by the above analysis it was possible to estimate the degree of functionalisation of the chain end. From the quantitative ^{13}C spectrum, the integration of the β-anomer carbon with respect to the polymer peaks in the region from δ 44.5 and 42.1 ppm gave a conversion of ~ 25 %. The integration was calculated after normalization to the polymer backbone peaks taking into account the 99% ^{13}C isotopic abundance of the β-anomer peak. This is shown in Equation 1, where the integrals refer to the peaks shown in Figure 4. The same result was obtained from ^{1}H-NMR by integration of β-anomer proton (δ 4.0 ppm) with respect to the polymer peaks in the region δ 1.5 and 1.2 ppm showed a conversion of 25 % (Figure S6).

$$Degree\ of\ conversion = \frac{I_{C1}}{\frac{\left(I_{(b+c+e+g)} * 99\right)}{52}} * 100 \quad (1)$$

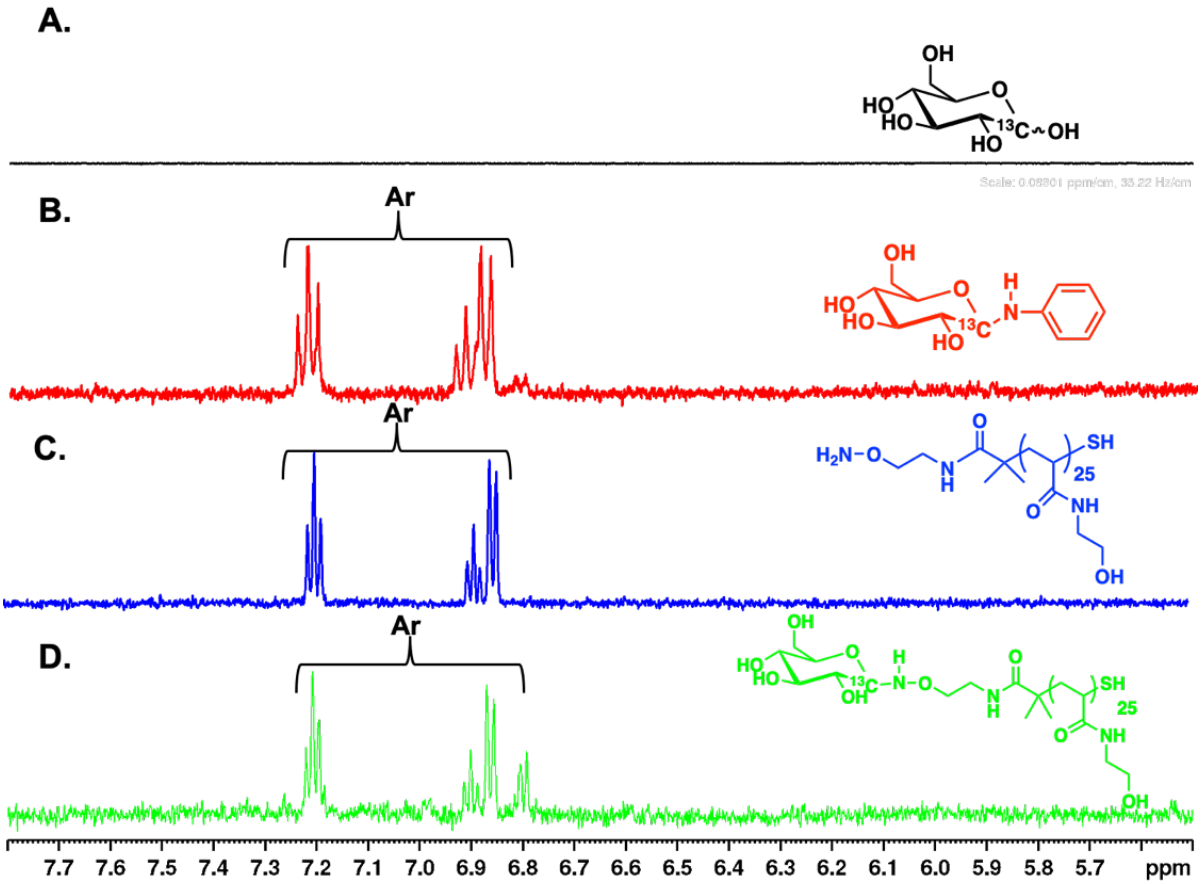

Figure 5. ^{1}H-NMR analysis of aromatic region during glycosylation. A) [1-^{13}C]-D-Glucose (black) in D_2O; B) [1-^{13}C]-D-Glucose in the reaction buffer (red); C) amino-oxy-$(pHEA)_{25}$ in reaction buffer without glucose (blue), D) amino-oxy-$pHEA_{25}$ glycosylation crude (green). The reaction solvent is acetate buffer 100 mM, aniline 1mM, D_2O pD =5.5.

Guided by the above studies showing the preferential formation of ring-closed structures, a panel of glycosylations were undertaken in acetate buffer (pH 5.5 plus aniline) with a library of eight reducing glycans: L-fucose (Fuc), *N*-acetyl-D-glucosamine (GlcNAc), D-mannose (Man), D-lactose (Lac), D-glucose (Glc), D-galactose (Gal), *N*-acetyl-D-galactosamine (GalNAc), 6'-sialyllactose sodium salt (6'SL) (Figure 6).

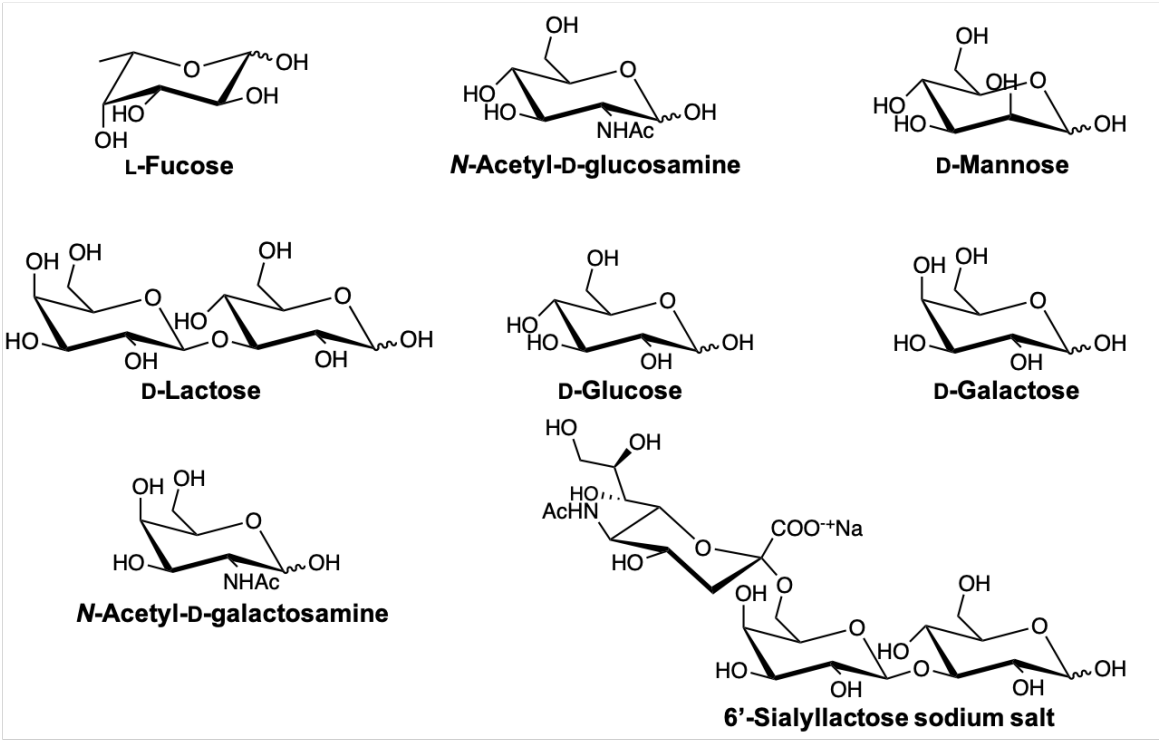

Figure 6. Reducing sugars conjugated to amino-oxy polymer.

The glycosylated polymers (which have residual glycan in solution) were not purified, but rather used directly in the next step to coat 20 nm citrate-stabilized gold nanoparticles. This is a crucial part of our strategy to simplify the process of obtaining glyconanomaterials. The glycopolymers (in buffer) were mixed with the nanoparticles dispersed in pure water. This step is essential as the citrate particles are not colloidally stable at pH 5.5 (the pH the glycosylation was undertaken in). Following this, excess glycan and polymer were removed by centrifugation and resuspension cycles. UV-visible spectroscopy[59] and dynamic light scattering (DLS) were used to characterize the particles (Figure 7A, 7B, Table S1 and Figure S8). There was a small bathochromic shift of the SPR band and an increase in hydrodynamic diameter of the particles to 33 nm, supportive of glycopolymers being grafted to the surface. The size of the nanoparticle cores was confirmed by transmission electron microscopy (TEM) of Glc-pHEA$_{25}$@Au$_{20}$ (Figure 7C and 7D) showing no aggregation or ripening (increased size) after functionalisation.

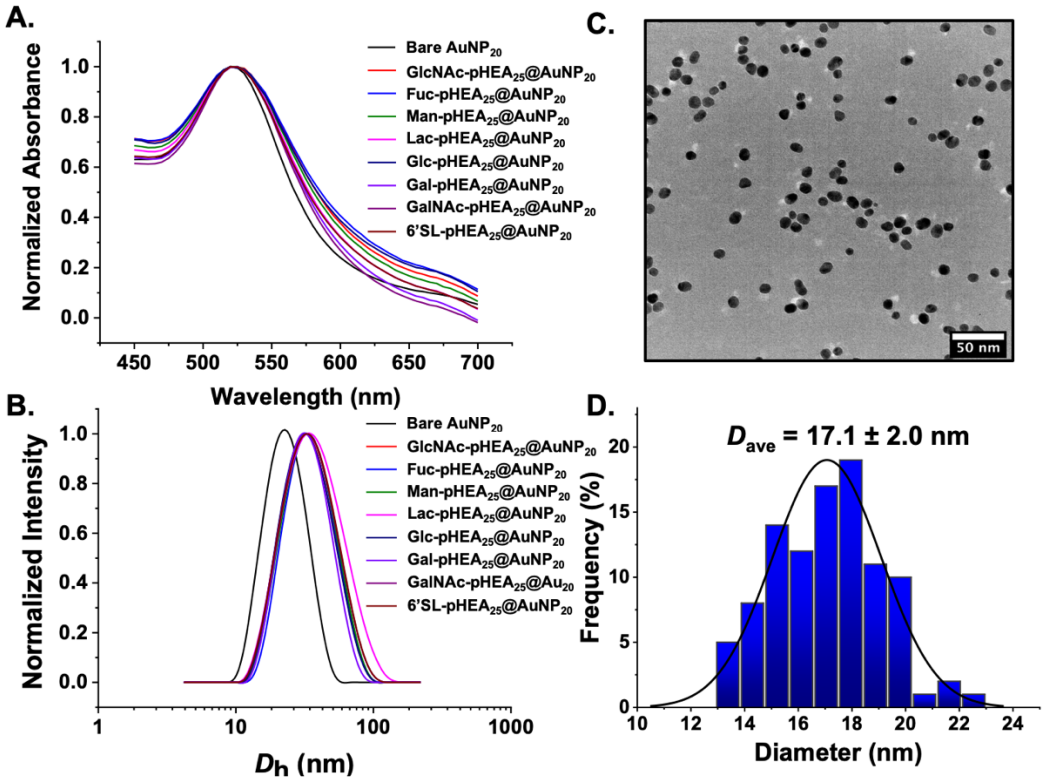

Figure 7. Glyconanoparticle characterization. A) UV-Vis spectra; B) Intensity-weighted DLS size distributions of glycopolymer-AuNPs; C) Representative dry-state TEM image of Glc-pHEA$_{25}$@Au$_{20}$; D) Histogram of particles size distribution measured from particle counting analysis from TEM images for Glc-pHEA$_{25}$@Au$_{20}$. In each case at least 100 particles were analyzed.

On spherical 20 nm gold nanoparticles grafting densities of ~ 0.3 chains nm^{-2} have been reported corresponding to sufficient numbers of glycans per particles to observe the cluster glycoside effect.[37,60] It is worth noting, however, that the 3-D presentation of glycans is equally important as the actual density/number in terms of generating high-affinity binders.[11,31,61] To provide further chemical information of the nanoparticle surfaces x-ray photoelectron spectroscopy (XPS) was employed (Figures S9 and S10, Supporting Info). The synthetic method developed here is intended to be compatible with the minute amounts (µg's) of material available for more complex glycans, where methods like NMR (as used in the model experiments above) are not sufficiently sensitive. Compared to the citrate-stabilized particles, there was a clear increase in both amide and ether (which includes -OH in the XPS-deconvolution method used) confirming polymer coating of the particles. Figure 8 shows

deconvoluted C 1*s* XPS spectra showing increased ether (including -OH) signals relative to amide when moving from amino-oxy to glycosylated polymer-coated particles confirming that glycans are present. Table 1 shows integrated values for each of the glyco-nanoparticles with an increase in ether:amide ratio in each case, consistent with glycosylation. Whilst XPS allows quantitative analysis, these were not converted into a % conversion due to the overlap in some of the peaks. But considering the 25 % conversion value obtained by $^{13}C/^{1}H$-NMR (above) a similar extent of glycosylation for each glycan type was obtained. Of note, the sialyllactose gave the highest ether:amide ratio but as it is a trisaccharide therefore the overall grafting is likely to be less (as each glycan brings 3 monosaccharide units per polymer and hence more OH groups) than the monosaccharides.

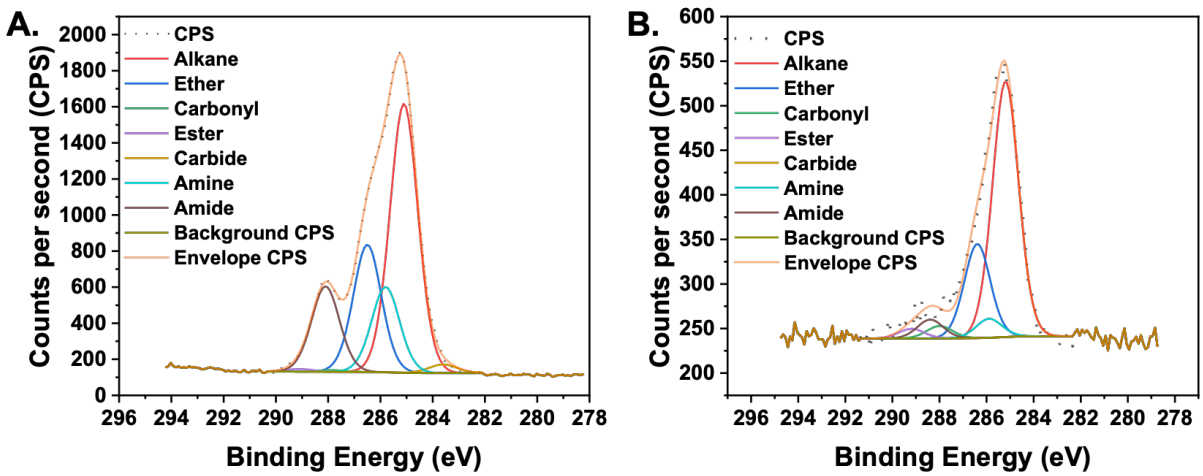

Figure 8. XPS C 1*s* characterization of A) $pHEA_{25}@Au_{20}$ and B) 6'-sialyllactose-$pHEA_{25}@Au_{20}$.

Table 1. XPS characterization of glyconanoparticles
Ether: Amide ratio was determined from integration of the C 1*s* peaks. Ether includes C-OH as well as C-O-C in the model used.

Particle Sample	Sugar	Particle composition (%)					
		Au 4*f*	C 1*s*	N 1*s*	O 1*s*	Au 4*f*:N 1*s*	Ether:Amide
Control Amino-oxy-pHEA$_{25}$	**No sugar**	0	66.42	9.93	23.65	0:100	1.49:1
Fuc-pHEA$_{25}$@Au$_{20}$	**Fuc**	2.11	40.74	1.46	55.69	59.08:40.92	3.50:1
GlcNAc-pHEA$_{25}$@Au$_{20}$	**GlcNAc**	2.82	46.66	1.30	49.22	68.52:31.48	3.07:1
Man-pHEA$_{25}$@Au$_{20}$	**Man**	3.37	40.46	2.22	53.95	60.24:39.76	4.19:1
Lac-pHEA$_{25}$@Au$_{20}$	**Lac**	4.24	50.57	2.06	43.13	67.24:32.76	3.57:1
Glc-pHEA$_{25}$@Au$_{20}$	**Glc**	3.90	38.92	1.94	55.25	66.75:33.25	3.08:1
GalNAc-pHEA$_{25}$@Au$_{20}$	**GalNAc**	3.83	37.48	2.01	56.68	65.59:34.41	2.96:1
Gal-pHEA$_{25}$@Au$_{20}$	**Gal**	3.63	44.15	1.91	50.31	65.52:34.48	3.67:1
6'-SL-pHEA$_{25}$@Au$_{20}$	**6'-SL**	1.92	38.37	1.75	57.96	52.32:47.68	4.96:1

Essentially all biomedical applications would require gold (or other) nanoparticles to be colloidally stable in relevant buffers. To this end, uncoated 20 nm AuNPs and the glyconanoparticle library were challenged with an NaCl gradient (31 mM – 1M) to change the ionic strength, mimicking biological systems (Figure S11, Supporting Info) and providing further evidence of steric stabilization. The citrate-coated (unfunctionalised) gold nanoparticles in the presence of salt aggregated and sedimented rapidly. In contrast all the polymer coated particles were stable at physiological saline concentrations (0.14 M NaCl). At higher NaCl concentrations (1M) there was some aggregation, but this concentration is far beyond what is observed in any application, but does helps establish a working range.

With this library of glyco-nanoparticles to hand, it was possible to screen for lectin binding. Initial studies attempted to use the red-blue colour shift associated with glyconanoparticle

binding to multivalent lectins, but the responses obtained were less than expected from previous reports with similar polymer-stabilised particles (Figure S12, Supporting Info).[37,46] As discussed above, ~ 25 % of the pHEA ligands are glycosylated using this strategy. It has been shown that lowering the glycan density (e.g. through tuning the polymer) can 'switch off' the aggregative response, whilst still have sufficient glycans on the surface to benefit from the cluster glycoside effect.[62] [It is also important to highlight that the aim of this method is to enable direct capture of reducing glycans, or those directly cleaved from proteins, which have no other functional handle for capture.] Therefore, biolayer interferometry was employed, to probe glycan binding to immobilised lectins. The BLI technique is similar to SPR and is able to afford label-free real time evaluation of binding interactions[45,63,64] between an immobilized ligand on the biosensor surface and the analyte in solution, by the change in the interference pattern of white light reflected from the surface of the biosensor. Lectins were biotinylated then captured onto streptavidin (SA) sensors. It should be noted that the total loading achieved for each lectin is different (but consistent in any series for each individual lectin) and hence the total binding capacity observed (below) will vary between them, but trends can be extracted, Figure 9. *Concanavalin A* (ConA) and *Wheat Germ Agglutinin* (WGA) which have a broad range of glycan specificities were employed as model lectins to demonstrate the glycans were available for binding.

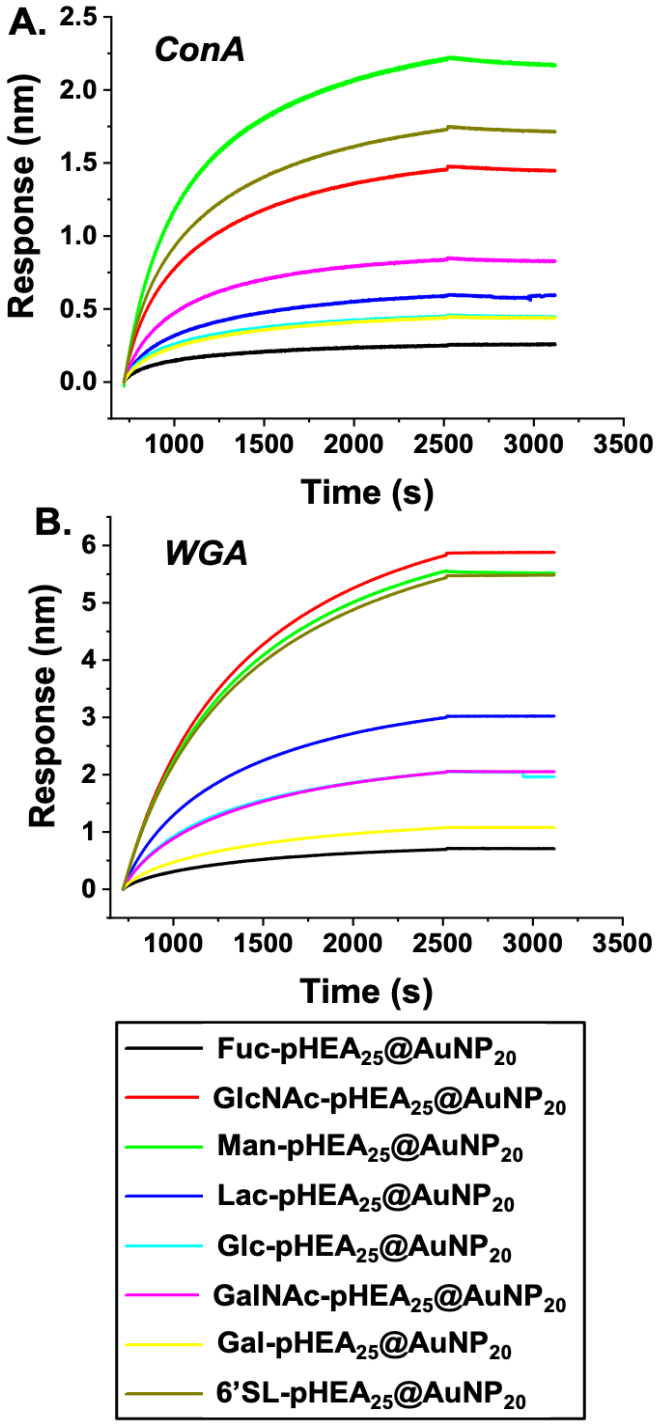

Figure 9. Biolayer interferometry analysis of particle/lectin binding. A) ConA functionalized BLI biosensors, B) WGA functionalized BLI biosensors.

ConA showed a preference for Man-pHEA$_{25}$@Au$_{20}$ as is expected for this lectin. [65] The other glyconanoparticles showed, in BLI, sequentially reduced affinity for the protein.[66] WGA is expected to show affinity towards *N*-acetyl-D-glucosamine (GlcNAc) with little or no anomeric preference between α- and β-glycosides and sialic acids.[67,68] BLI confirmed that GlcNAc-

pHEA$_{25}$@Au$_{20}$ and 6'-SL-pHEA$_{25}$@Au$_{20}$ showed more binding in comparison to the other glyconanoparticles. In *N*-acetyl-D-glucosamine and 6'-sialyllactose sodium salt the *N*-acetamide and its vicinal hydroxyl groups are both in equatorial position which contribute to WGA binding.[67] Surprisingly, Man-pHEA$_{25}$@Au$_{20}$ displayed an affinity similar to 6'SL-pHEA$_{25}$@Au$_{20}$, but some cross-reactivity in multivalent platforms is not unexpected.

Overall, our findings provide a facile synthetic strategy to enable the assembly of glyconanoparticles without requiring multi-step oligosaccharide synthesis and may be suitable for high-throughput evaluations of glycomaterial-protein interactions, particularly initial screening studies where high-densities of the glycan may not be essential to map out new binding interactions.

CONCLUSIONS

In summary, we present a convergent synthetic approach for the capture of reducing glycans, without any protecting group manipulations, in aqueous solution, onto polymer ligands which are then used to coat AuNPs producing multivalent glyconanoparticles. Crucially, this methodology is conducted with practicality in mind, with no need for complex purification, with any excess glycans/polymers removed by simple centrifugation cycles. To enable capture of the glycans, amino-oxy terminated poly(*N*-hydroxyethyl acrylamide) was synthesized by RAFT polymerization *via* a pentafluoro-phenol-terminated precursor. This polymer choice is crucial, as it is fully water soluble to enable capture of the glycans by the amino-oxy group in acetate buffer; for more complex glycans, only aqueous solvents are suitable. Following ligand exchange on the surface of gold particles, glyconanoparticles were obtained by centrifugation and characterized by a range of methods to prove capture of the glycans and the polymer onto the surface. A ^{13}C-NMR study using isotope-labelled glucose showed that ~ 25 % of polymer chains are glycosylated, which must be considered in subsequent binding analyses and in comparisons of affinity measurements. To demonstrate that the glycans were available for lectin binding, biolayer interferometry was used to evaluate the interactions against a panel of model lectins. Despite the localization on the polymer end-group and the unnatural linkage arising from the amino-oxy conjugation, the particles retained their expected binding specificities. This simple approach for capture of glycans will find application in the assembly of libraries of glyconanoparticles, as each step is also ideal for automation, with the normally challenging glycosylation step made easy, with no protecting groups and simple purification.

EXPERIMENTAL SECTION

Additional synthetic and characterization details are included in Supporting Information (SI)

Materials

All chemicals were used as supplied unless otherwise stated. 1-Dodecanethiol (≥98%), 2-bromo-2-methylpropionic acid (98%), carbon disulfide (anhydrous, ≥99%), tripotassium phosphate (≥98%), pentafluorophenol (≥99%), 4-(dimethylamino)pyridine (≥98%, DMAP), *N*-hydroxyethyl acrylamide (97%, HEA), triethylamine (>99%), sodium citrate tribasic dihydrate (>99%), gold(III) chloride trihydrate (99.9%), ammonium carbonate (reagent grade), diisopropyl azodicarboxylate (98%), hydrazine hydrate (50-60%), *N*-hydroxyphthalimide (97%), *N*-Boc-ethanolamine (98%), triphenylphosphine (99%) and aniline (≥99.5%) were all purchased from Sigma-Aldrich. Sodium acetate anhydrous (99%) and acetic acid (glacial) (>99%) were purchased from Fisher Scientific. *N*-(3-dimethylaminopropyl)-*N*'-ethylcarbodiimide hydrochloride (EDC·HCl), L-fucose (≥99%), *N*-acetyl-D-glucosamine (≥99%), *N*-acetyl-D-galactosamine (≥99%) and 6'-sialyllactose sodium salt (≥99%) were all purchased from Carbosynth. D-Glucose-1-^{13}C (99 atom % ^{13}C), D-mannose (≥99%), D-lactose monohydrate (≥98%), D-glucose (≥99.5%), D-galactose (≥98%) were purchased from Sigma-Aldrich. Streptavidin (SA) biosensors were purchased from Forte Bio. Concanavalin A (ConA) and wheat germ agglutinin (WGA) were purchased from Sigma Aldrich. Soybean agglutinin (SBA) was purchased from Vector Labs. Lectins were biotinylated using EZ-Link Sulfo-NHS-LC-Biotin reagent from Thermo Fisher Scientific using standard procedure (20-fold molar excess of biotin reagent, conjugation performed in PBS buffer and isolated using Amicon Ultra-0.5 mL 3000 MWCO centrifugal filters from Merck Millipore). 100 mM acetate buffer (pH 5.5) and 10 mM HEPES buffer containing 50 mM NaCl, 0.1 mM $CaCl_2$ and 0.01 mM $MnCl_2$ (pH 7.5) were prepared respectively in 200 mL and 1 L of pure water. Phosphate-buffered saline (PBS) solution was prepared using pre-formulated tablets (Sigma-Aldrich) in

200 mL of pure water yielding 10 mM phosphate buffer, 2.7 mM KCl, and 137 mM NaCl. Clear and black half 96-well plates were purchased from Greiner Bio-one. Formvar coated copper grids were purchased from EM Resolutions.

Physical and Analytical Methods.

Centrifugations were performed with a Thermo Scientific Heraeus Multifuge X1 Centrifuge instrument at 25 °C (7000 rpm, 10 min). Dialyses were conducted on Spectra/Por 1.0 kDa, 3.5 kDa MWCO membranes at 25 °C. Freeze-drying was performed with a Christ Alpha 1-4 LD plus freeze-dryer.

NMR Spectroscopy. NMR spectra were recorded on a Bruker DRX-400 (^{1}H: 400 MHz, ^{13}C: 100 MHz) and on a Bruker DRX-600 (^{1}H: 400 MHz, ^{13}C: 150 MHz) instruments, in D_2O (acetone as internal standard, ^{1}H: $(CH_3)_2CO$ at δ 2.22 ppm; ^{13}C: $(CH_3)_2CO$ at δ 31.5 ppm) or $CDCl_3$ (^{1}H: $CHCl_3$ at δ 7.24 ppm; ^{13}C: $CDCl_3$ at δ 77.23 ppm). HSQC experiment was measured in the ^{1}H-detected mode by single quantum coherence with proton decoupling in the ^{13}C domain, by using data sets of 1024X128 points and typically 128 increments.

Size Exclusion Chromatography. Size exclusion chromatography (SEC) analysis was performed on an Agilent Infinity II MDS instrument equipped with differential refractive index (DRI), viscometry (VS), dual angle light scatter (LS) and variable wavelength UV detectors. The system was equipped with 2 x PLgel Mixed D columns (300 x 7.5 mm) and a PLgel 5 µm guard column. The mobile phase used was DMF (HPLC grade) containing 5 mM NH_4BF_4 at 50 °C at flow rate of 1.0 mL.min^{-1}. Poly(methyl methacrylate) (PMMA) standards (Agilent EasyVials) were used for calibration between 955,000 – 550 g.mol^{-1}. Analyte samples were filtered through a nylon membrane with 0.22 μm pore size before injection. Number average molecular weights (M_n), weight average molecular weights (M_w) and dispersities ($Đ_M = M_w/M_n$)

were determined by conventional calibration and universal calibration using Agilent GPC/SEC software.

FT-IR Spectroscopy. Infrared absorptions were recorded on a Bruker Alpha FT-IR spectrometer using a Golden Gate diamond attenuated total reflection cell in the range of 650 to 4000 cm^{-1}.

UV-Vis Spectroscopy. Absorbance measurements were recorded on an Agilent Cary 60 UV-Vis Spectrophotometer and on a BioTek Epoch microplate reader.

Dynamic Light Scattering. Hydrodynamic diameters (D_h) and size distributions of particles were determined in water solution by dynamic light scattering (DLS) using a Malvern Zetasizer Nano ZS with a 4 mW He-Ne 633 nm laser module operating at 25 °C. Measurements were carried out at an angle of 173° (back scattering), and results were analyzed using Malvern DTS 7.03 software. All determinations were repeated 5 times with at least 10 measurements recorded for each run. D_h values were calculated using the Stokes-Einstein equation where particles are assumed to be spherical.

Transmission Electron Microscopy. Dry-state TEM imaging was performed on a JEOL JEM-2100Plus microscope operating at an acceleration voltage of 200 kV. All dry-state samples were diluted with deionized water and then deposited onto formvar-coated copper grids.

X-ray Photoelectron Spectroscopy. The x-ray photoelectron spectroscopy (XPS) data was collected at the Warwick Photoemission Facility, University of Warwick. The samples were attached to electrically-conductive carbon tape, mounted on to a sample bar and loaded in to a Kratos Axis Ultra DLD spectrometer which possesses a base pressure below 1×10^{-10} mbar. Measurements were performed in the main analysis chamber, with the sample being illuminated using a monochromated Al Kα x-ray source. The measurements were conducted at room temperature and at a take-off angle of 90° with respect to the surface parallel. The core

level spectra were recorded using a pass energy of 20 eV (resolution approx. 0.4 eV), from an analysis area of 300 μm x 700 μm. The spectrometer work function and binding energy scale of the spectrometer were calibrated using the Fermi edge and $3d_{5/2}$ peak recorded from a polycrystalline Ag sample prior to the commencement of the experiments. In order to prevent surface charging the surface was flooded with a beam of low energy electrons throughout the experiment and this necessitated recalibration of the binding energy scale. To achieve this, the C-C/C-H component of the C 1*s* spectrum was referenced to 285.0 eV. The data was analyze d in the CasaXPS package, using Shirley backgrounds and mixed Gaussian-Lorentzian (Voigt) lineshapes. For compositional analysis, the analyzer transmission function has been determined using clean metallic foils to determine the detection efficiency across the full binding energy range.

Synthetic procedures

Synthesis of 2-((tert-butyl *N*-2-aminoethyl)carbamate)-isoindole-1,3-dione (1).

N-hydroxyphthalimide (1.98 g, 12.16 mmol) was suspended in THF (20 mL), treated with *N*-Boc-ethanolamine (1.88 mL, 12.16 mmol) and PPh_3 (3.33 g, 12.70 mmol). The suspension was cooled to 0˚C and DIAD (2.46 mL, 12.70 mmol) was dropwise added. The yellow solution was left warming to R.T. and stirred for ~19 h. The crude was concentrated under reduced pressure and further purified by flash column chromatography (Hexane-Ethyl Acetate 2:1 → 1:1) obtaining **1** as white crystals (4.96 g, 50% purity), but contaminated by diisopropyl hydrazine-1,2-dicarboxylate.

ESI-MS: 306.1 (M+H)

^{1}H-NMR (methanol-d_4): δ (ppm) = 7.82 (m, 4H, H-Ar), 4.18 (d, 2H, CH_2CH$_2$NHCO), 3.37 (m, 2H, CH$_2$CH_2NHCO), 1.41 (s, 9H C(CH_3)$_3$)

^{1}H-NMR (DMSO-d_6): δ (ppm) = 7.87 (m, 4H, H-Ar), 6.83 (s, 1H, CH_2CH_2NHCO), 4.12 (m, 2H, CH_2CH_2NHCO), 3.26 (m, 2H, CH_2CH_2NHCO), 1.38 (s, 9H $C(CH_3)_3$)

^{13}C-NMR (methanol-d_4): δ (ppm) = 167.1, 136.4, 129.7, 124.6 (Phthalimide), 156.2 ($COC(CH_3)_3$), 77.1 (CH_2CH_2NHCO), 39.3 (CH_2CH_2NHCO), 27.9 ($C(CH_3)_3$).

^{13}C-NMR (DMSO-d_6): δ (ppm) = 165.1, 135.4, 127.7, 123.5 (Phthalimide), 164.2 ($COC(CH_3)_3$), 78.1 (CH_2CH_2NHCO), 39.7 (CH_2CH_2NHCO), 28.0 ($C(CH_3)_3$).

Synthesis of 2-(2-amino-ethoxy)-isoindole-1,3-dione hydrochloride (2).

Compound **1** (4.96 g) was suspended in EtOAc (2 mL) and treated with 4 M HCl solution in EtOAc and left stirred at room temperature for 2 h, obtaining compound **2** (2.48 g, quantitative) as a white solid that was collected by centrifugation which was used in the next step without any further purification.

ESI-MS: 445.3 (2 Amine + MeOH + H), 477.3 (2 Amine + 2 MeOH + H)

^{1}H-NMR (methanol-d_4): δ (ppm) = 7.93-7.84 (m, 4H, H-Ar), 4.43 (m, 2H, $CH_2CH_2NH_3$), 3.34 (m, 2H, $CH_2CH_2NH_3$)

^{1}H-NMR (DMSO-d_6): δ (ppm) = 8.30 (s, 3H, $CH_2CH_2NH_3$), 7.88 (m, 4H, H-Ar), 4.36 (m, 2H, $CH_2CH_2NH_3$), 3.16 (m, 2H, $CH_2CH_2NH_3$)

^{13}C-NMR (methanol-d_4): δ (ppm) = 165.5, 136.5, 130.4, 124.8 (Phthalimide), 75.6 ($CH_2CH_2NH_3$), 39.8 ($CH_2CH_2NH_3$)

^{13}C-NMR (DMSO-d_6): δ (ppm) = 163.5, 135.3, 128.5, 123.5 (Phthalimide), 73.7 ($CH_2CH_2NH_3$), 36.4 ($CH_2CH_2NH_3$)

Post-polymerization modification of poly (*N*-hydroxyethylacrylamide) with 2-(2-amino-ethoxy)-isoindole-1,3-dione hydrochloride.

PFP-pHEA$_{25}$ polymer (0.100 g, 0.032 mmol) was dissolved in DMF (5 mL), treated with **2** (0.040 g, 0.164 mmol) and Et_3N (100 µL), stirring all at T = 50 ˚C overnight. The dark yellow

solution was cooled to room temperature and diethyl ether (20 mL) as precipitating agent was added, obtaining 2-(2-amino-ethoxy)-isoindole-1,3-dione-pHEA$_{25}$ post-modified polymer (0.0788 g, 80.3 %) as a brown solid that was collected by centrifugation and dried under vacuum. Successful attachment of compound **2** on polymer and removal of the PFP group confirmed by ^{1}H-NMR, ^{19}F-NMR and FT-IR analysis.

Removal of phthaloyl protecting group.

Phthalimide-terminated pHEA$_{25}$ polymer (0.0788 g, 0.026 mmol) was dissolved in DMF (5 mL) and treated with $N_2H_4 \cdot H_2O$ 50-60% (5 mL, 50 mmol) and left stirred overnight at T = 50 ˚C. A change in the colour of the solution was observed and the crude was diluted with H_2O (25 mL), dialyzed and freeze-dried, affording amino-oxy-terminated pHEA$_{25}$ polymer.

General procedure for glycosylation.

Solutions of amino-oxy terminated pHEA$_{25}$ polymer (0.001 g, 0.343 μmol) were treated with 20 eq of glycans and dissolved in 100 mM acetate buffer (pH 5.5) with presence of 1 mM aniline (500 μL) and the solution was heated at T = 50 ˚C overnight. The obtained 1 mg/mL solution was used for coating on gold nanoparticles without any further purification.

Functionalization of gold nanoparticles.

1 mg.mL^{-1} of polymer solution was added to 1 mL of 20 nm particles and was left stirred at room temperature for 30 minutes. The particle solution was centrifuged at 4600 x g, the supernatant with any unattached polymer was removed and then the particles were resuspended in water and then characterized by UV-Vis, DLS and TEM in the same conditions used for the unfunctionalized gold nanoparticles.

CONFLICTS OF INTEREST

There are no conflicts to declare.

DATA ACCESS STATEMENT

The background data sets for this work are available from wrap.warwick.ac.uk

ACKNOWLEDGEMENTS

MIG holds an ERC starting grant (CRYOMAT 638661). SJR is supported by the Specialty Glycans project form the BBSRC/Innovate UK BB/M02878X/1. The BBSRC-funded MIBTP program (BB/M01116X/1) and Iceni Diagnostics ltd are also thanked for a studentship for AB. AL holds a Royal Society – CNR International Fellowship (NF170965). This project has received funding from the European Union's Horizon 2020 research and innovation programme under the Marie Skłodowska-Curie grant agreement No 814236. Dr. Ivan Prokes (UoW) is thanked for the assistance with NMR spectroscopic measurements. The Warwick Polymer Research Technology Platform is acknowledged for SEC analysis, and Warwick Electron Microscopy Research Technology Platform is acknowledged for TEM.

Supporting Information.

Supporting information is available free of charge from the ACS webpages. This includes additional synthetic protocols, NMR spectra, XPS spectra and additional AuNP characterization data.

REFERENCES

(1) Lundquist, J. J., and Toone, E. J. (2002) The Cluster Glycoside Effect. *Chem. Rev. 102*, 555–578. https://doi.org/10.1021/cr000418f.

(2) Bertozzi, C. R., Kiessling, and L., L. (2001) Chemical Glycobiology. *Science 291*, 2357–2364. https://doi.org/10.1126/science.1059820.

(3) Sigal, G. B., Mammen, M., Dahmann, G., and Whitesides, G. M. (1996) Polyacrylamides Bearing Pendant α-Sialoside Groups Strongly Inhibit Agglutination of Erythrocytes by Influenza Virus: The Strong Inhibition Reflects Enhanced Binding through Cooperative Polyvalent Interactions. *J. Am. Chem. Soc. 118*, 3789–3800. https://doi.org/10.1021/ja953729u.

(4) Ambrosi, M., Cameron, N. R., and Davis, B. G. (2005) Lectins: Tools for the Molecular Understanding of the Glycocode. *Org. Biomol. Chem. 3*, 1593–1608. https://doi.org/10.1039/b414350g.

(5) Wu, L., Zhang, Y., Li, Z., Yang, G., Kochovski, Z., Chen, G., and Jiang, M. (2017) "sweet" Architecture-Dependent Uptake of Glycocalyx-Mimicking Nanoparticles Based on Biodegradable Aliphatic Polyesters by Macrophages. *J. Am. Chem. Soc. 139*, 14684–14692. https://doi.org/10.1021/jacs.7b07768.

(6) Jones, M. W., Otten, L., Richards, S.-J., Lowery, R., Phillips, D. J., Haddleton, D. M., and Gibson, M. I. (2014) Glycopolymers with Secondary Binding Motifs Mimic Glycan Branching and Display Bacterial Lectin Selectivity in Addition to Affinity. *Chem. Sci. 5*, 1611–1616. https://doi.org/10.1039/c3sc52982g.

(7) Bernardi, A., Jiménez-Barbero, J., Casnati, A., De Castro, C., Darbre, T., Fieschi, F., Finne, J., Funken, H., Jaeger, K.-E., Lahmann, M., et al. (2013) Multivalent Glycoconjugates as Anti-Pathogenic Agents. *Chem. Soc. Rev. 42*, 4709–4727. https://doi.org/10.1039/c2cs35408j.

(8) Kiessling, L. L., Gestwicki, J. E., and Strong, L. E. (2006) Synthetic Multivalent Ligands as Probes of Signal Transduction. *Angew. Chemie - Int. Ed. 45*, 2348–2368. https://doi.org/10.1002/anie.200502794.

(9) Kumar, V., and Turnbull, W. B. (2018) Carbohydrate Inhibitors of Cholera Toxin. *Beilstein Journal of Organic Chemistry*. Beilstein-Institut 2018, pp 484–498. https://doi.org/10.3762/bjoc.14.34.

(10) Branson, T. R., and Turnbull, W. B. (2013) Bacterial Toxin Inhibitors Based on Multivalent Scaffolds. *Chem. Soc. Rev. 42*, 4613–4622. https://doi.org/10.1039/c2cs35430f.

(11) Richards, S.-J., Jones, M. W., Hunaban, M., Haddleton, D. M., and Gibson, M. I. (2012) Probing Bacterial-Toxin Inhibition with Synthetic Glycopolymers Prepared by Tandem Post-Polymerization Modification: Role of Linker Length and Carbohydrate Density. *Angew. Chemie - Int. Ed. 51*, 7812–7816. https://doi.org/10.1002/anie.201202945.

(12) Sharon, N. (2006) Carbohydrates as Future Anti-Adhesion Drugs for Infectious Diseases. *Biochim. Biophys. Acta - Gen. Subj. 1760*, 527–537.

https://doi.org/10.1016/j.bbagen.2005.12.008.

(13) Mammen, M., Dahmann, G., and Whitesides, G. M. (1995) Effective Inhibitors of Hemagglutination by Influenza Virus Synthesized from Polymers Having Active Ester Groups. Insight into Mechanism of Inhibition. *J. Med. Chem. 38*, 4179–4190. https://doi.org/10.1021/jm00021a007.

(14) Jarvis, C. M., Zwick, D. B., Grim, J. C., Alam, M. M., Prost, L. R., Gardiner, J. C., Park, S., Zimdars, L. L., Sherer, N. M., and Kiessling, L. L. (2019) Antigen Structure Affects Cellular Routing through DC-SIGN. *Proc. Natl. Acad. Sci. 116*, 14862–14867. https://doi.org/10.1073/pnas.1820165116.

(15) Zhang, S., Moussodia, R.-O., Vértesy, S., André, S., Klein, M. L., Gabius, H.-J., and Percec, V. (2015) Unraveling Functional Significance of Natural Variations of a Human Galectin by Glycodendrimersomes with Programmable Glycan Surface. *Proc. Natl. Acad. Sci. U. S. A. 112*, 5585–5590. https://doi.org/10.1073/pnas.1506220112.

(16) Ponader, D., Maffre, P., Aretz, J., Pussak, D., Ninnemann, N. M., Schmidt, S., Seeberger, P. H., Rademacher, C., Nienhaus, G. U., and Hartmann, L. (2014) Carbohydrate-Lectin Recognition of Sequence-Defined Heteromultivalent Glycooligomers. *J. Am. Chem. Soc. 136*, 2008–2016. https://doi.org/10.1021/ja411582t.

(17) Mitchell, D. A., Zhang, Q., Voorhaar, L., Haddleton, D. M., Herath, S., Gleinich, A. S., Randeva, H. S., Crispin, M., Lehnert, H., Wallis, R., et al. (2017) Manipulation of Cytokine Secretion in Human Dendritic Cells Using Glycopolymers with Picomolar Affinity for DC-SIGN. *Chem. Sci. 8*, 6974–6980. https://doi.org/10.1039/c7sc01515a.

(18) Rillahan, C. D., and Paulson, J. C. (2011) Glycan Microarrays for Decoding the Glycome. *Annu. Rev. Biochem. 80*, 797–823. https://doi.org/10.1146/annurev-biochem-061809-152236.

(19) Feizi, T., Fazio, F., Chai, W., and Wong, C. H. (2003) Carbohydrate Microarrays - a New Set of Technologies at the Frontiers of Glycomics. *Curr. Opin. Struct. Biol. 13*, 637–645.

(20) Park, S., Lee, M. R., and Shin, I. (2009) Construction of Carbohydrate Microarrays by Using One-Step, Direct Immobilizations of Diverse Unmodified Glycans on Solid Surfaces. *Bioconjug. Chem. 20*, 155–162. https://doi.org/10.1021/bc800442z.

(21) Park, S., Lee, M. R., and Shin, I. (2007) Fabrication of Carbohydrate Chips and Their Use to Probe Protein-Carbohydrate Interactions. *Nat. Protoc. 2*, 2747–2758. https://doi.org/10.1038/nprot.2007.373.

(22) Palma, A. S., Feizi, T., Childs, R. A., Chai, W., and Liu, Y. (2014) The Neoglycolipid (NGL)-Based Oligosaccharide Microarray System Poised to Decipher the Meta-Glycome. *Curr. Opin. Chem. Biol. 18*, 87–94. https://doi.org/10.1016/j.cbpa.2014.01.007.

(23) Ambrosi, M., Batsanov, A. S., Cameron, N. R., Davis, B. G., Howard, J. A. K., and Hunter, R. (2002) Influence of Preparation Procedure on Polymer Composition: Synthesis and Characterisation of Polymethacrylates Bearing β-D-Glucopyranoside and β-D-Galactopyranoside Residues. *J. Chem. Soc. Perkin 1 2*, 45–52. https://doi.org/10.1039/b108421f.

(24) Gauthier, M. A., Gibson, M. I., and Klok, H.-A. (2009) Synthesis of Functional Polymers by Post-Polymerization Modification. *Angew. Chemie - Int. Ed. 48*, 48–58. https://doi.org/10.1002/anie.200801951.

(25) Ladmiral, V., Mantovani, G., Clarkson, G. J., Cauet, S., Irwin, J. L., and Haddleton, D. M. (2006) Synthesis of Neoglycopolymers by a Combination of "Click Chemistry" and Living Radical Polymerization. *J. Am. Chem. Soc. 128*, 4823–4830. https://doi.org/10.1021/ja058364k.

(26) Chen, G., Amajjahe, S., and Stenzel, M. H. (2009) Synthesis of Thiol-Linked Neoglycopolymers and Thermo-Responsive Glycomicelles as Potential Drug Carrier. *Chem. Commun.* No. 10, 1198. https://doi.org/10.1039/b900215d.

(27) Semsarilar, M., Ladmiral, V., and Perrier, S. (2010) Highly Branched and Hyperbranched Glycopolymers via Reversible Addition−Fragmentation Chain Transfer Polymerization and Click Chemistry. *Macromolecules 43*, 1438–1443. https://doi.org/10.1021/ma902587r.

(28) Boyer, C., Bousquet, A., Rondolo, J., Whittaker, M. R., Stenzel, M. H., and Davis, T. P. (2010) Glycopolymer Decoration of Gold Nanoparticles Using a LbL Approach. *Macromolecules 43*, 3775–3784. https://doi.org/10.1021/ma100250x.

(29) Jones, M. W., Richards, S.-J., Haddleton, D. M., and Gibson, M. I. (2013) Poly(Azlactone)s: Versatile Scaffolds for Tandem Post-Polymerisation Modification and Glycopolymer Synthesis. *Polym. Chem. 4*, 717–723. https://doi.org/10.1039/c2py20757e.

(30) Gibson, M. I., Fröhlich, E., and Klok, H.-A. (2009) Postpolymerization Modification of Poly(Pentafluorophenyl Methacrylate): Synthesis of a Diverse Water-Soluble Polymer Library. *J. Polym. Sci. Part A Polym. Chem. 47*, 4332–4345. https://doi.org/10.1002/pola.23486.

(31) Wilkins, L. E., Badi, N., Du Prez, F., and Gibson, M. I. (2018) Double-Modified Glycopolymers from Thiolactones to Modulate Lectin Selectivity and Affinity. *ACS Macro Lett. 7*, 1498–1502. https://doi.org/10.1021/acsmacrolett.8b00825.

(32) Lim, D., Brimble, M. A., Kowalczyk, R., Watson, A. J. A., and Fairbanks, A. J. (2014) Protecting-Group-Free One-Pot Synthesis of Glycoconjugates Directly from Reducing Sugars. *Angew. Chem. Int. Ed. 53*, 11907–11911. https://doi.org/10.1002/anie.201406694.

(33) Tanaka, T., Nagai, H., Noguchi, M., Kobayashi, A., and Shoda, S. I. (2009) One-Step Conversion of Unprotected Sugars to β-Glycosyl Azides Using 2-Chloroimidazolinium Salt in Aqueous Solution. *Chem. Commun.* 3378–3379. https://doi.org/10.1039/b905761g.

(34) Bernardes, G. J. L., Gamblin, D. P., and Davis, B. G. (2006) The Direct Formation of Glycosyl Thiols from Reducing Sugars Allows One-Pot Protein Glycoconjugation. *Angew. Chem. Int. Ed. 45*, 4007–4011. https://doi.org/10.1002/anie.200600685.

(35) Guberman, M., and Seeberger, P. H. (2019) Automated Glycan Assembly: A Perspective. *J. Am. Chem. Soc. 141*, 5581–5592. https://doi.org/10.1021/jacs.9b00638.

(36) Liu, L. H., and Yan, M. (2010) Perfluorophenyl Azides: New Applications in Surface Functionalization and Nanomaterial Synthesis. *Acc. Chem. Res. 43*, 1434–1443.

https://doi.org/10.1021/ar100066t.

(37) Richards, S.-J., Otten, L., Besra, G. S., and Gibson, M. I. (2016) Glycosylated Gold Nanoparticle Libraries for Label-Free Multiplexed Lectin Biosensing. *J. Mater. Chem. B 4*, 3046–3053. https://doi.org/10.1039/C5TB01994J.

(38) Crisan, D. N., Creese, O., Ball, R., Brioso, J. L., Martyn, B., Montenegro, J., and Fernandez-Trillo, F. (2017) Poly(Acryloyl Hydrazide), a Versatile Scaffold for the Preparation of Functional Polymers: Synthesis and Post-Polymerisation Modification. *Polym. Chem. 8*, 4576–4584. https://doi.org/10.1039/c7py00535k.

(39) Godula, K., and Bertozzi, C. R. (2010) Synthesis of Glycopolymers for Microarray Applications via Ligation of Reducing Sugars to a Poly(Acryloyl Hydrazide) Scaffold. *J. Am. Chem. Soc. 132*, 9963–9965. https://doi.org/10.1021/ja103009d.

(40) Mahon, C. S., Fascione, M. A., Sakonsinsiri, C., McAllister, T. E., Turnbull, W. B., and Fulton, D. A. (2015) Templating Carbohydrate-Functionalised Polymer-Scaffolded Dynamic Combinatorial Libraries with Lectins. *Org. Biomol. Chem. 13*, 2756–2761. https://doi.org/10.1039/c4ob02587c.

(41) Pifferi, C., Daskhan, G. C., Fiore, M., Shiao, T. C., Roy, R., and Renaudet, O. (2017) *Aminooxylated Carbohydrates: Synthesis and Applications*; Vol. 117, pp 9839–9873. https://doi.org/10.1021/acs.chemrev.6b00733.

(42) Kalia, J., and Raines, R. T. (2008) Hydrolytic Stability of Hydrazones and Oximes. *Angew. Chemie - Int. Ed. 47*, 7523–7526. https://doi.org/10.1002/anie.200802651.

(43) Goff, R. D., and Thorson, J. S. (2014) Neoglycosylation and Neoglycorandomization: Enabling Tools for the Discovery of Novel Glycosylated Bioactive Probes and Early Stage Leads. *Medchemcomm 5*, 1036–1047. https://doi.org/10.1039/c4md00117f.

(44) Godula, K., and Bertozzi, C. R. (2012) Density Variant Glycan Microarray for Evaluating Cross-Linking of Mucin-like Glycoconjugates by Lectins. *J. Am. Chem. Soc. 134*, 15732–15742. https://doi.org/10.1021/ja302193u.

(45) Richards, S.-J., Baker, A. N., Walker, M., and Gibson, M. I. (2020) Polymer-Stabilized Sialylated Nanoparticles: Synthesis, Optimization, and Differential Binding to Influenza Hemagglutinins. *Biomacromolecules 21*, 1604–1612. https://doi.org/10.1021/acs.biomac.0c00179.

(46) Richards, S.-J., and Gibson, M. I. (2014) Optimization of the Polymer Coating for Glycosylated Gold Nanoparticle Biosensors to Ensure Stability and Rapid Optical Readouts. *ACS Macro Lett. 3*, 1004–1008. https://doi.org/10.1021/mz5004882.

(47) Xu, J., He, J., Fan, D., Wang, X., and Yang, Y. (2006) Aminolysis of Polymers with Thiocarbonylthio Termini Prepared by RAFT Polymerization: The Difference between Polystyrene and Polymethacrylates. *Macromolecules 39*, 8616–8624. https://doi.org/10.1021/ma061961m.

(48) von der Ehe, C., Weber, C., Gottschaldt, M., and Schubert, U. S. (2016) Immobilized Glycopolymers: Synthesis, Methods and Applications. *Prog. Polym. Sci. 57*, 64–102. https://doi.org/https://doi.org/10.1016/j.progpolymsci.2016.02.001.

(49) Grünewald, J., Jin, Y., Vance, J., Read, J., Wang, X., Wan, Y., Zhou, H., Ou, W., Klock, H. E., Peters, E. C., et al. (2017) Optimization of an Enzymatic Antibody–Drug Conjugation Approach Based on Coenzyme A Analogs. *Bioconjug. Chem. 28*, 1906–

1915. https://doi.org/10.1021/acs.bioconjchem.7b00236.

(50) Mitsunobu, O., and Yamada, M. (1967) Preparation of Esters of Carboxylic and Phosphoric Acid via Quaternary Phosphonium Salts. *Bull. Chem. Soc. Jpn. 40*, 2380–2382. https://doi.org/10.1246/bcsj.40.2380.

(51) Villadsen, K., Martos-Maldonado, M. C., Jensen, K. J., and Thygesen, M. B. (2017) Chemoselective Reactions for the Synthesis of Glycoconjugates from Unprotected Carbohydrates. *ChemBioChem*. John Wiley & Sons, Ltd April 4, 2017, pp 574–612. https://doi.org/10.1002/cbic.201600582.

(52) Thygesen, M. B., Munch, H., Sauer, J., Cló, E., Jørgensen, M. R., Hindsgaul, O., and Jensen, K. J. (2010) Nucleophilic Catalysis of Carbohydrate Oxime Formation by Anilines. *J. Org. Chem. 75*, 1752–1755. https://doi.org/10.1021/jo902425v.

(53) Kenneth Ladner, H., Led, J. J., and Grant, D. M. (1975) Deuterium Isotope Effects on 13C Chemical Shifts in Amino Acids and Dipeptides. *J. Magn. Reson. 20*, 530–534. https://doi.org/10.1016/0022-2364(75)90010-4.

(54) Coxon, B. (2005) Deuterium Isotope Effects in Carbohydrates Revisited. Cryoprobe Studies of the Anomerization and NH to ND Deuterium Isotope Induced 13C NMR Chemical Shifts of Acetamidodeoxy and Aminodeoxy Sugars. *Carbohydr. Res. 340*, 1714–1721. https://doi.org/10.1016/j.carres.2005.04.022.

(55) Gudmundsdottir, A. V., Paul, C. E., and Nitz, M. (2009) Stability Studies of Hydrazide and Hydroxylamine-Based Glycoconjugates in Aqueous Solution. *Carbohydr. Res. 344*, 278–284. https://doi.org/10.1016/j.carres.2008.11.007.

(56) Peri, F., Dumy, P., and Mutter, M. (1998) Chemo- and Stereoselective Glycosylation of Hydroxylamino Derivatives: A Versatile Approach to Glycoconjugates. *Tetrahedron 54*, 12269–12278. https://doi.org/10.1016/S0040-4020(98)00763-7.

(57) Baudendistel, O. R., Wieland, D. E., Schmidt, M. S., and Wittmann, V. (2016) Real-Time NMR Studies of Oxyamine Ligations of Reducing Carbohydrates under Equilibrium Conditions. *Chem. - A Eur. J. 22*, 17359–17365. https://doi.org/10.1002/chem.201603369.

(58) Bridiau, N., Benmansour, M., Legoy, M. D., and Maugard, T. (2007) One-Pot Stereoselective Synthesis of β-N-Aryl-Glycosides by N-Glycosylation of Aromatic Amines: Application to the Synthesis of Tumor-Associated Carbohydrate Antigen Building Blocks. *Tetrahedron 63*, 4178–4183. https://doi.org/10.1016/j.tet.2007.02.092.

(59) Haiss, Wolfgang; Thanh, N. T. K. ., Aveyard, J. and, and Fernig, D. G. (2007) Determination of Size and Concentration of Gold Nanoparticles from UV−Vis Spectra. *Anal. Chem. 79*, 4215–4221. https://doi.org/10.1021/AC0702084.

(60) Klok, H.-A., Gibson, M. I., and Paripovic, D. (2010) Size-Dependent LCST Transitions of Polymer-Coated Gold Nanoparticles: Cooperative Aggregation and Surface Assembly. *Adv. Mater. 22*, 4721–4725. https://doi.org/10.1002/adma.201001382.

(61) Reynolds, M., Marradi, M., Imberty, A., Penadés, S., and Pérez, S. (2013) Influence of Ligand Presentation Density on the Molecular Recognition of Mannose-Functionalised Glyconanoparticles by Bacterial Lectin BC2L-A. *Glycoconj. J. 30*, 747–757.

https://doi.org/10.1007/s10719-013-9478-6.

(62) Georgiou, P. G., Baker, A. N., Richards, S. J., Laezza, A., Walker, M., and Gibson, M. I. (2020) Tuning Aggregative versus Non-Aggregative Lectin Binding with Glycosylated Nanoparticles by the Nature of the Polymer Ligand. *J. Mater. Chem. B 8*, 136–145. https://doi.org/10.1039/c9tb02004g.

(63) Rich, R. L., and Myszka, D. G. (2007) Higher-Throughput, Label-Free, Real-Time Molecular Interaction Analysis. *Analytical Biochemistry*. 2007, pp 1–6. https://doi.org/10.1016/j.ab.2006.10.040.

(64) Laigre, E., Goyard, D., Tiertant, C., Dejeu, J., and Renaudet, O. (2018) The Study of Multivalent Carbohydrate–Protein Interactions by Bio-Layer Interferometry. *Org. Biomol. Chem. 16*, 8899–8903. https://doi.org/10.1039/C8OB01664J.

(65) Goldstein, I. J., Winter, H. C., and Poretz, R. D. (1997) Plant Lectins: Tools for the Study of Complex Carbohydrates. In *New Comprehensive Biochemistry*; Elsevier; Vol. 29, pp 403–474. https://doi.org/10.1016/S0167-7306(08)60625-0.

(66) Cummings, R. D., Darvill, A. G., Etzler, M. E., and Hahn, M. G. (2015) Glycan-Recognizing Probes as Tools. In *Essentials of Glycobiology*; Cold Spring Harbor Laboratory Press. https://doi.org/10.1101/GLYCOBIOLOGY.3E.048.

(67) Monsigny, M., Roche, A.-C., Sene, C., Maget-Dana, R., and Delmotte, F. (1980) Sugar-Lectin Interactions: How Does Wheat-Germ Agglutinin Bind Sialoglycoconjugates? *Eur. J. Biochem. 104*, 147–153. https://doi.org/10.1111/j.1432-1033.1980.tb04410.x.

(68) Van Damme, J. M.; Peumans, W. J.; Pusztai, A.; Bardocz, S. (1997) Handbook of Plant Lectins: Properties and Biomedical Applications. In *Artocarpus integrifolia (also known as A. heterophyllus)*; Wiley; pp 120–123.